International Journal of Bifurcation and Chaos, Vol. 29, No. 12 (2019) 1930035 (17 pages)

DOI: 10.1142/S0218127419300350

Robust Hyperbolic Chaos in Froude Pendulum with Delayed Feedback and Periodic Braking

Sergey P. Kuznetsov[*,†,‡] and Yuliya V. Sedova[†,§]
[*]*Udmurt State University, Universitetskaya 1, Izhevsk, 426034, Russian Federation*
[†]*Kotel'nikov's Institute of Radio-Engineering and Electronics of RAS, Saratov Branch, Zelenaya 38, Saratov, 410019, Russian Federation*
[‡]*spkuz@yandex.ru*
[§]*sedovayv@yandex.ru*

Received April 15, 2019

We indicate a possibility of implementing hyperbolic chaos using a Froude pendulum that is able to produce self-oscillations due to the suspension on a shaft rotating at constant angular velocity, in the presence of time-delay feedback and of periodic braking by the application of additional frictional force. We formulate a mathematical model and carry out its numerical research. In the parameter space we reveal areas of chaotic and regular dynamics using the analysis of Lyapunov exponents and some other diagnostic tools. It is shown that there are regions in the parameter space where the Poincaré stroboscopic map has an attractor, which is a kind of Smale–Williams solenoid embedded in the infinite-dimensional state space. We confirm the hyperbolicity of the attractor by numerical calculations including the analysis of angles of intersections of stable and unstable invariant subspaces of vectors of small perturbations for trajectories on the attractor and verify the absence of tangencies between these subspaces.

Keywords: Chaos; hyperbolicity; Smale–Williams solenoid; Froude pendulum; time-delay; self-oscillations.

1. Introduction

In this paper, we propose a new example of a nonautonomous mechanical system, manifesting chaotic dynamics associated with the Smale–Williams solenoid, which refers to the category of structurally stable hyperbolic attractors [Smale, 1967; Anosov *et al.*, 1995; Katok & Hasselblatt, 1995; Shilnikov, 1997].

The considered system is based on the Froude pendulum, known as a classic example of self-oscillations, which take place due to the suspension of the pendulum on a shaft rotating at constant angular velocity [Rayleigh & Lindsay, 1945; Strelkov, 1933; Rabinovich & Trubetskov, 2012; Landa, 2013; Dai & Singh, 1998; Cao *et al.*, 2004]. We consider the Froude pendulum, supplemented by the time-delay feedback and by periodic braking caused by the application of additional friction force.

A characteristic feature of pendulum systems is that they are characterized by a particular nonlinearity, given by the sine function. Besides mechanics, systems with such nonlinearity occur in other areas of physics as well. For example, in electronics, these are Josephson junctions [Likharev, 1986] and phase-locked loop devices [Best, 2007]. A generalization to the case of distributed systems with such nonlinearity is the famous sine-Gordon equation, which is being studied intensively in the context of numerous diverse tasks [Cuevas-Maraver *et al.*, 2014]. In relation to all these problems, considerations of analogs built on the base of the

mechanical object, the pendulum, are very productive for understanding complex dynamical behaviors, since they appeal to intuitively clear representations, interpretation and visualization for the mechanical systems.

Uniformly hyperbolic attractors are characterized by the property of roughness or structural stability, which is why they persist under small variations of the system parameters [Anosov *et al.*, 1995; Katok & Hasselblatt, 1995; Shilnikov, 1997; Pugh & Peixoto, 2008]. This property referred to as robustness is highly desirable for chaos applications [Banerjee *et al.*, 1998; Elhadj & Sprott, 2011; Dmitriev *et al.*, 2012; Gusso *et al.*, 2019]. As it is well known, the robust chaos contrasts with the "fragile chaos", most often taking place in dynamical systems, which is associated with quasi-attractors [Shilnikov, 1997]. In the latter case, the dynamical behavior observed in numerical calculations or in experiments, although it looks chaotic, is characterized by the presence along with the chaotic trajectories also of regular attracting sets ("sinks") with narrow basins of attraction in the same region of phase space, or they appear under small parameter variations.

Design of systems with hyperbolic attractors requires special efforts, and until recently, well-known examples were limited to mathematical constructions. One such example is the Smale–Williams solenoid [Smale, 1967; Anosov *et al.*, 1995; Katok & Hasselblatt, 1995; Shilnikov, 1997; Kuznetsov, 2011, 2012].

Let in the phase space of some abstract dynamical system for a certain time interval, a region in the form of torus filled with points representing instantaneous states, undergo stretching in the longitudinal direction twice, and strong transverse compression, and folding into a loop placed inside the original torus, as shown in Fig. 1. At each iteration, the volume of the object decreases, and the number of coils doubles. The limit object is solenoid, which has an infinite number of coils and possesses Cantor structure in transversal cross-section. The essential point is that one of the dynamical variables, the angular coordinate φ, undergoes in one step of the construction a transformation of such topological nature that one round of the full circle for the preimage corresponds to a double round for the image. The dynamics of individual representative points that evolve in accordance with this rule (it is called the Bernoulli map) is chaotic. Although the described scheme appeals for clarity to the three-dimensional state space, this moment is not of principal significance, and attractors of the same type can occur in state spaces of higher dimensions as well.

According to the mathematical theory [Smale, 1967; Anosov *et al.*, 1995; Katok & Hasselblatt, 1995; Shilnikov, 1997], a hyperbolic attractor is composed of saddle-type trajectories, at which the vectors of infinitely small perturbations can be represented by linear combinations of vectors of contracting and expanding invariant subspaces. The first subspace is a set of vectors whose norms decrease exponentially in the course of evolution in direct time, and the second is a set of vectors whose norms decrease exponentially in reverse time. The sets of orbits approaching a given trajectory in direct or inverse time correspond, respectively, to the stable and unstable manifolds of this

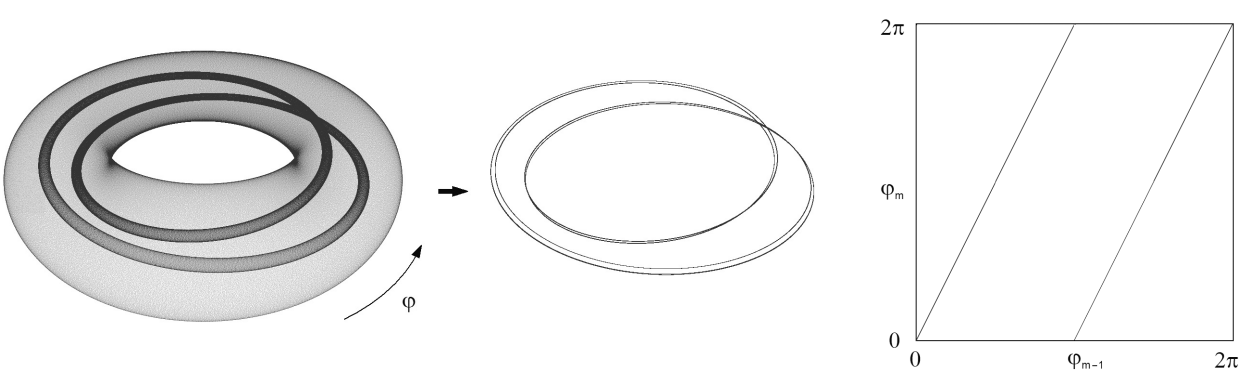

Fig. 1. (a) Transformation of a region in the form of torus in one evolution step in time and a limit object, the solenoid attractor and (b) a plot of the angular coordinate for a point on the attractor at time step m as a function of the previous value at $m - 1$.

trajectory. For a hyperbolic attractor, these manifolds can intersect, but cannot have tangencies.

In Sec. 2, we introduce the modification of the Froude pendulum to be studied and obtain the dynamic equations describing this system. In Sec. 3, we discuss some properties of the classical Froude pendulum important for understanding the occurrence of hyperbolic chaos in the modified system. Namely, we outline the dependence of the self-oscillation frequency on the amplitude when the parameter of activity is varied; we outline a possibility of self-oscillations of frequency at half of the natural frequency of small oscillations. In Sec. 4, we explain the principle of operation of our system with time-delay feedback and periodic braking of the pendulum, which makes it possible for the Smale–Williams solenoid attractor to occur in the map describing the transformation of the state on successive periods of the parameter modulation. Also we present numerical results of modeling dynamics of the system including waveforms, pictures of attractors, and Lyapunov exponents. The key point of confirming the nature of the attractor as the Smale–Williams solenoid, is plotting the diagrams, illustrating transformation of the angular variable (the oscillation phase at the activity stage), where one complete circle round for a preimage corresponds to a double round for the image. In Sec. 5, we discuss how the system dynamics depend on parameters, in particular, we present charts of regimes manifesting areas of hyperbolic and non-hyperbolic chaos, and regions of regular regimes. In Sec. 6, we discuss the method and results of verifying the hyperbolicity of attractors by means of the "angle criterion" adapted for the time-delay system, based on the analysis of the intersection angles of stable and unstable invariant subspaces of the trajectories belonging to the attractor, revealing the absence of tangencies of these manifolds (hyperbolicity) or the presence of the tangencies (no hyperbolicity).

2. The System Studied and Main Equations

A well-known example of mechanical self-oscillations is the Froude pendulum [Rayleigh & Lindsay, 1945; Strelkov, 1933; Rabinovich & Trubetskov, 2012; Landa, 2013; Dai & Singh, 1998]. Let us turn to the modified version of such a pendulum, which will be our main subject of study, see Fig. 2.

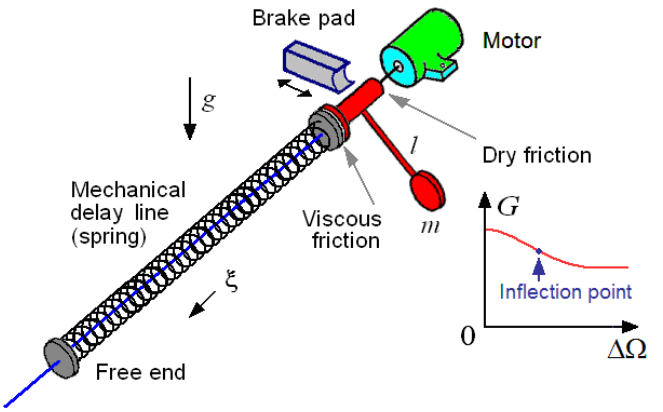

Fig. 2. Froude pendulum, where self-oscillations are ensured due to the rotation of the shaft on which the sleeve attached to the pendulum is placed, and the corresponding plot of dependence of the dry friction force on the relative angular velocity. The system is supplemented with a mechanical time-delay line (spring) and a mechanism providing alternate braking and excitation of the oscillations.

Suppose we have a rod of length l, at one end of which a weight of mass m is fixed, and the other end is attached to a sleeve placed on a shaft rotating at constant angular velocity Ω. The equation of motion of the pendulum is

$$ml^2\ddot{x} + \alpha(t)\dot{x} + mgl\sin x = G(\Omega - \dot{x}) + M(t), \quad (1)$$

where x is the pendulum angle away from the vertical, g is the gravity acceleration constant, and α is a coefficient of viscous friction, which in our formulation of the problem will vary in time due to periodic application of the brake pad. The moment of the force of dry friction between the shaft and the sleeve $G(\Delta\Omega)$ is assumed to decrease depending on the relative angular velocity, also we suppose application of external force moment $M(t)$ provided by some device introducing the time-delay feedback. As such a device, an electromechanical controller may be used, but the simplest option (say, for an experimental implementation) is a mechanical time-delay transmission line such as a spring of length L, which at one end comes into contact with the pendulum with viscous friction, while the second end is left free (Fig. 2).

Let us derive the equations describing action of the time-delay line on the pendulum. Let ξ be coordinate counted along the transmission line, $J\Delta\xi$ be the moment of inertia of the spring section of length $\Delta\xi$, $k/\Delta\xi$ be the stiffness coefficient of the

section $\Delta\xi$. The equations describing the propagation of the torsion waves in the spring transmission line have the form

$$J\frac{\partial\omega}{\partial t} = -\frac{\partial M}{\partial\xi}, \quad \frac{\partial M}{\partial t} = -k\frac{\partial\omega}{\partial\xi}, \tag{2}$$

where $\omega(t,\xi)$ is the instantaneous local angular velocity of the spring element, and $M(t,\xi)$ is the local moment of force acting on the spring element.

For the speed c of the wave propagation in the spring transmission line and the constant ρ, which is the mechanical wave impedance, we have

$$c = \sqrt{kJ^{-1}}, \quad \rho = \sqrt{kJ}, \tag{3}$$

and the general solution of Eqs. (2) is written as

$$\begin{aligned} M(t,\xi) &= f_1\left(t-\frac{\xi}{c}\right) + f_2\left(t+\frac{\xi}{c}\right), \\ \omega(t,\xi) &= \rho^{-1}\left[f_1\left(t-\frac{\xi}{c}\right) - f_2\left(t+\frac{\xi}{c}\right)\right], \end{aligned} \tag{4}$$

where f_1 and f_2 are arbitrary functions.

In the presence of viscous friction at the point of contact with the pendulum, which has an instantaneous angular velocity $\dot{x}$, we should write down $M(t,0) = \kappa[\dot{x}(t) - \omega(t,0)]$ at the end, $\xi = 0$, of the transmission line, or $f_1(t) + f_2(t) = \kappa\dot{x} - \kappa\rho^{-1}f_1(t) + \kappa\rho^{-1}f_2(t)$, where κ is the friction coefficient. We confine ourselves here to considering the case of no-reflection load, when $\kappa = \rho$. Then an explicit expression for the function is obtained, $f_1(t) = \frac{1}{2}\rho\dot{x}(t)$. Further, the free boundary condition $M(t,L) = 0$ at the other end of the time-delay line $\xi = L$ is reduced to $f_1(t - L/c) + f_2(t + L/c) = 0$, so that $f_2(t) = -f_1(t - 2L/c)$. Therefore, for the friction force moment acting on the pendulum from the spring, we obtain $M(t) = -M(t,0) = -f_1(t) - f_2(t)$, or

$$M(t) = \frac{1}{2}\rho\left[\dot{x}\left(t-\frac{2L}{c}\right) - \dot{x}(t)\right]. \tag{5}$$

As often assumed in the theoretical analysis of the Froude pendulum [Dai & Singh, 1998; Cao *et al.*, 2004; Landa, 2013], let us suppose that the function $G(\Delta\Omega)$ characterizing the friction between the sleeve and the shaft is represented by decreasing the function with inflection point, and the rotation speed of the shaft is chosen corresponding to the inflection point. Then the Taylor decomposition of the function near this point is

$$\begin{aligned} G(\Omega - \dot{x}) &\approx G(\Omega) - G'(\Omega)\dot{x} - \frac{1}{6}G'''(\Omega)\dot{x}^3 \\ &= G_0 + A\dot{x} - B\dot{x}^3. \end{aligned} \tag{6}$$

As a result, under the assumptions made, Eq. (1) takes a form

$$\begin{aligned} ml^2\ddot{x} + [\alpha(t) - A + B\dot{x}^2]\dot{x} + mgl\sin x \\ = G_0 + \frac{1}{2}\rho\left[\dot{x}\left(t-\frac{2L}{c}\right) - \dot{x}(t)\right]. \end{aligned} \tag{7}$$

When introducing the dimensionless quantities

$$\begin{aligned} t' = \omega_0 t = t\sqrt{\frac{g}{l}}, \quad d = \frac{\alpha}{ml^2\omega_0}, \\ a = \frac{A}{ml^2\omega_0}, \quad b = \frac{B\omega_0}{ml^2}, \\ \mu = \omega_0^{-2}G_0, \quad \varepsilon = \frac{\rho}{2ml^2\omega_0}, \quad \tau = \frac{2L\omega_0}{c}, \end{aligned} \tag{8}$$

we come to the equation

$$\begin{aligned} \ddot{x} + [d(t) - a + b\dot{x}^2]\dot{x} + \sin x \\ = \mu + \varepsilon[\dot{x}(t-\tau) - \dot{x}], \end{aligned} \tag{9}$$

where a dot means a derivative with respect to the dimensionless time. (For brevity, the prime in notation of the dimensionless time is omitted here and later.) The coefficient $d(t)$ in the equation will be assigned to be zero without braking, and to be a constant $D > 0$ when the brake pad is applied periodically for time interval T_0 with period T. Specifically, we set

$$d(t) = \begin{cases} 0, & t < T_0, \\ D, & T_0 < t < \dfrac{T}{2}, \\ 0, & \dfrac{T}{2} < t < T, \end{cases} \quad d(t+T) = d(t). \tag{10}$$

3. On Froude Pendulum Without Braking and Time-Delay

Let us return for a while to the conventional Froude pendulum, without braking and time-delay feedback involved. This is the case $d(t) = \text{const}$, $\varepsilon = 0$,

so the problem is described by an ordinary second-order differential equation

$$\ddot{x} + (d - a + b\dot{x}^2)\dot{x} + \sin x = \mu. \qquad (11)$$

In such a reduced system, chaos is impossible, but we will discuss briefly this system in one relevant aspect, following [Kuznetsov & Kruglov, 2019].

If $a - d > 0$, then in the system (11) self-oscillations arise represented on the phase plane by a limit cycle going around the equilibrium state O, $(x, \dot{x}) = (\arcsin\mu, 0)$. At small amplitudes, the frequency of the self-oscillations is close to the natural oscillator frequency $f = (2\pi)^{-1}$. With increasing $a-d$ the limit cycle grows in size, and the frequency f decreases. This is due to the fact that as the maximum angular deviation of the pendulum becomes closer and closer to the unstable upside down pendulum position, the point of the saddle S $(x, \dot{x}) = (\pi - \arcsin\mu, 0)$, along the motion of the phase trajectories slows down. A further increase of the parameter leads to a transition from the oscillatory motions to periodic rotational movements of the pendulum, which correspond to limit cycles bypassing the phase cylinder, and their frequencies are much higher. Figure 3(a) shows limit cycles corresponding to sustained regimes of the Froude pendulum (11) at $b = 0.16$, $\mu = 0.087$ for different values of $a - d$, and Fig. 3(b) presents a plot of the frequency of the self-oscillations versus this parameter.

Note a possibility of choosing parameters in such a way that the frequency of self-oscillations becomes equal exactly to a half of the frequency of small oscillations. For example, at $\mu = 0.087$, $b = 0.16$, this takes place at $a - d = 0.360$. The process of the large-amplitude relaxation oscillations contains a significant second harmonic, so that action of the generated signal on a linear oscillator with unit natural frequency is accompanied with its resonance buildup stimulated by the second harmonic of the self-oscillator [Fig. 3(c)].

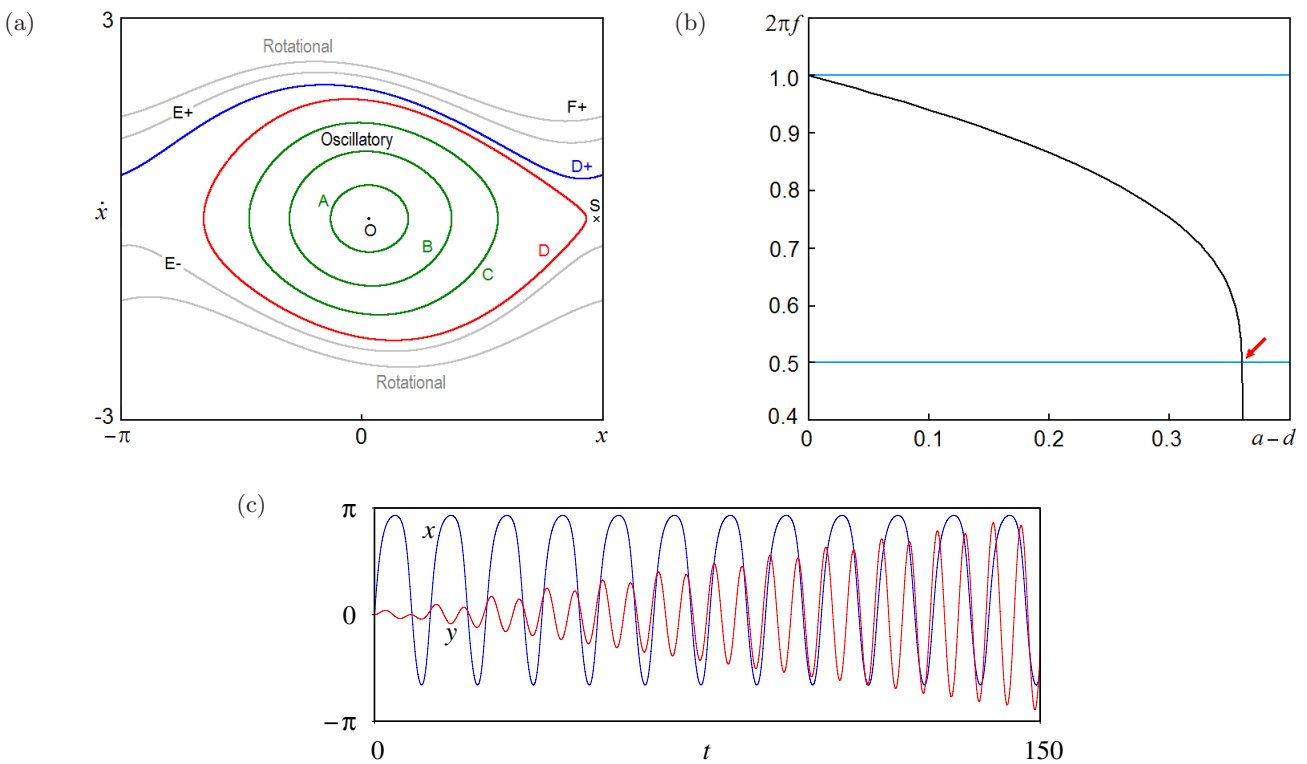

Fig. 3. Attracting limit cycles for various parameters corresponding to sustained periodic motions of the Froude pendulum: (a) Oscillatory A, B, C, D at $a - d = 0.03, 0.12, 0.24, 0.36$, with frequencies $2\pi f = 0.982, 0.926, 0.827, 0.50$, and rotational $D+$, $E\pm$, $F\pm$, at $a - d = 0.36, 0.48, 0.60$, with frequencies $1.201(D+), 1.622(E+), 1.044(E-)$, $1.88(F+), 1.66(F-)$. (b) The dependence of the frequency of self-oscillations on the parameter $a - d$. The arrow shows the situation, which corresponds to the frequency of half of the frequency of small oscillations of the pendulum. (c) The resonant buildup of a linear oscillator under the action of the second harmonic of the self-oscillating system according to the results of numerical integration of equations $\ddot{x} - (a - b\dot{x}^2)\dot{x} + \sin x = \mu, \ddot{y} + y = \varepsilon\dot{x}$ with parameters $a = 0.36$, $b = 0.16$, $\mu = 0.087$, $\varepsilon = 0.06$.

In [Kuznetsov & Kruglov, 2019], this observation was used to construct a system with the Smale–Williams attractor consisting of two Froude pendulums, which are excited turn by turn due to alternating periodic braking, so that the parameter controlling the activity in one and the other subsystem is characterized by the presence of a plateau of the time dependence at the level corresponding to the desired value of the frequency of the relaxation self-oscillations. In the present paper, we show that, with the same success, a similar type of attractor can be obtained for a single pendulum with alternating excitation and suppression of the oscillations, if we add the time-delay feedback. (A similar approach to systems based on the Bonhoeffer–van der Pol oscillator was developed in [Doroshenko *et al.*, 2018; Kuznetsov & Sedova, 2019].)

4. The Mechanism of Appearance of Hyperbolic Chaos and Numerical Results

Let us consider again the Froude pendulum modification introduced in Sec. 2 with time-delay feedback and periodic switching of linear dissipation on and off by attaching the brake pad providing damping of the self-oscillations.

It is important to note that the system governed by Eqs. (9) and (10), in contrast to the reduced system (11), is characterized by an infinite dimension of the phase space, like other systems with time-delay [Bellman & Cooke, 2012; El'sgol'ts & Norkin, 1973; Farmer, 1982; Yanchuk & Giacomelli, 2017]. Indeed, in order to determine unambiguously the subsequent evolution of the system in time with certain initial conditions, along with the quantities x and $\dot{x}$ at some instant t_0, it is also necessary to set the function $\dot{x}(t_0 - \tau)$ on the time interval of duration τ.

Within the framework of the problem statement discussed in Sec. 2, this corresponds to the fact that in addition to the instantaneous values of the deflection angle and the angular velocity of the pendulum at the initial time moment, we should take into account also an instantaneous state of the transmission line characterized by some distribution of momentums and angular velocities of the spring coils along its length.

Our system is nonautonomous, with periodic parameter modulation, so we can use the description of the dynamics in terms of discrete time by means of the stroboscopic Poincaré map

$$\mathbf{X}_n = \mathbf{F}_T(\mathbf{X}_{n-1}). \tag{12}$$

Here vectors $\mathbf{X}_n$ denote the sets of quantities $x(t_n)$, $\dot{x}(t_n)$ together with functions $\dot{x}(t-\tau)$, $t \in [t_n - \tau, t_n)$ determining the state of the system at the time instants $t_n = nT$, and should be interpreted as elements of the infinite-dimensional state space.

In this section, the parameters of the model (9) and (10) will be assigned as follows:

$$a = 0.36, \quad b = 0.16, \quad \mu = 0.087, \quad \varepsilon = 0.0003,$$
$$D = 0.8, \quad T = 250, \quad T_0 = \frac{T}{4}, \quad \tau = \frac{T}{2}. \tag{13}$$

Let us explain the mechanism of the system functioning, which is responsible for the appearance of the Smale–Williams attractor in the Poincaré map. Let us start with a situation when the braking is not applied, and the pendulum performs relaxation self-oscillations, in which, due to the mentioned selection of the parameters, the frequency is half of that for the small oscillations of the pendulum. The signal generated at this stage is sent to the time-delay feedback transmission line. Further, the pendulum oscillations are damped by the application of the brake pad. When braking stops, a new stage of the buildup of the oscillations begins, starting from the practically unexcited state of the pendulum. As we properly select the delay time, the progress of the oscillatory process will be stimulated by resonant action of the second harmonic of the signal received through the feedback circuit and emitted just on the previous stage of intense oscillations. Therefore, the phase of the developing oscillations corresponds to the doubled phase of the main component of oscillations at the prior activity stage. As a result, when the newly arisen oscillations of the pendulum approach the sustained relaxation self-oscillations, their phase will be doubled compared to the phase at the preceding activity stage. Further, the process is repeated again and again. A full cycle corresponding to the modulation period T is accompanied by multiplxying the initial phase of the oscillatory process by two, i.e. for it, a doubly expanding circle map takes place. Due to compression in the remaining directions in the state space of the map $\mathbf{X}_n = \mathbf{F}_T(\mathbf{X}_{n-1})$, the Smale–Williams attractor arises.

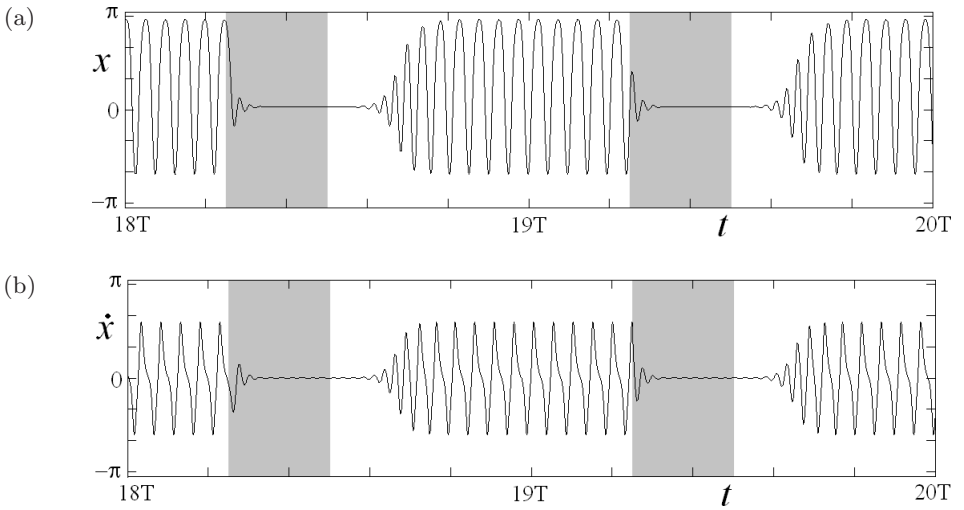

Fig. 4. Waveforms for the pendulum deflection $x(t)$ and the angular velocity $\dot{x}(t)$ in the regime of hyperbolic chaos plotted according to the results of numerical integration of Eq. (9) with parameters (13). The gray bands correspond to the time intervals where the pendulum is subjected to the brake pad application.

Let us turn to the illustrations of the functioning of the system based on the results of numerical simulation. To integrate Eq. (9), the Runge–Kutta method of order four was used, adapted for the time-delay system. The values of variables and functions at each step of the difference scheme are accumulated as an array that contains data for the previous time interval τ. In the process of calculations the delayed values of these quantities are to be substituted, and this data array is accessed.

Figure 4 shows typical waveforms of the pendulum angular coordinate and velocity obtained by numerical integration of Eq. (9) in sustained regime; it illustrates the idea of the functioning of the system in accordance with the above mechanism. To make visible the main oscillatory process, we have shown a relatively short time interval. Although it gives no opportunity to judge confidently about the chaotic nature of the dynamics, one can note that relative positions of the oscillation forms do not repeat themselves at successive activity stages relative to the time intervals of the braking application.

Before turning to other illustrations that definitely indicate the chaotic nature of this regime and reveal hyperbolicity of the corresponding attractor, we need to make a notion concerning the numerical evaluation of the phases of the oscillations. In the domain of developed self-oscillations, their shape differs significantly from the sinusoidal one; therefore, a simple calculation of the phases through arctangent of the ratio of the variable and its derivative does not lead to satisfactory results. An alternative is to use a value that determines a time shift relative to a certain origin normalized to the characteristic period of the self-oscillations. Let t be the moment of the termination of the braking of the pendulum, and t_1 and t_2 are the preceding moments of reaching the maximums of the angular velocity $\dot{x}$ of the pendulum. Then, we can define the phase as a variable belonging to the interval $[0, 1]$ according to the relation $\varphi = \frac{t-t_2}{t_2-t_1}$. In the process of numerical modeling of the system dynamics, the phase is evaluated at the end of each next stage of activity.

Figure 5(a) shows a diagram for the phases obtained in numerical calculations for a sufficiently large number of main periods. As one can see, topologically the mapping for the phases looks equivalent to the Bernoulli map $\varphi_{n+1} = 2\varphi_n + \text{const} \pmod 1$; indeed, one passage of the full unit interval

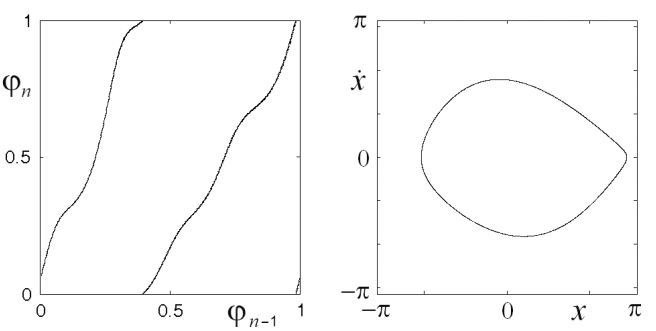

Fig. 5. Diagram for phases of oscillations at successive periods of activity of the oscillator in system (9) and the portrait of the attractor for the stroboscopic Poincaré map in projection on the plane of variables $(x, \dot{x})$. Parameters are assigned in accordance with (13).

for the preimage corresponds to a double passage for the image.

Figure 5(b) shows the attractor of the Poincaré stroboscopic map. It should be interpreted as a projection of the Smale–Williams solenoid from the infinite-dimensional state space of the time-delay system on the plane. The object looks like a closed curve, but in fact it has a thin structure of filaments (indistinguishable because of high degree of transversal compression of the phase volume). A representative point does not move along the "curve", but jumps at a step of evolution in such way that the angular variable follows the chaotic map.

The chaotic nature of the dynamics is confirmed by forms of power density spectra, which are shown in Fig. 6. The spectra were obtained by processing time series for the deflection angle and the angular velocity of the pendulum from numerical integration of Eq. (9) using the method of statistical evaluation of the spectral density of random processes [Jenkins & Watts, 1968; Sveshnikov, 2014]. Namely, the time series is divided into sections of certain duration (it determines the inverse value of the frequency resolution of the analysis), followed by multiplying the fragments of the time series by the window function (for improving the quality of spectral analysis preventing the effect of widening of spectral components caused by mismatch of signal levels at the edges of the split intervals). Next, Fourier transformation is performed for each of the intervals, and the squares of the amplitudes of the spectral components are averaged over the acceptable set of the intervals.

From Fig. 6 it can be seen that the spectra have a continuous component, like those for random processes. A set of discrete lines in the left parts of the graphs is due to a presence of the periodic parameter modulation in the system. In the considered regime, the modulation period is $T = 250$, so the distance between the spectral lines is $\Delta f = T^{-1} = 0.004$ in correspondence with that observed on the graph. Widened peaks in the spectra correspond to the main frequency of relaxation oscillations at the activity stage $f \approx (4\pi)^{-1} \approx 0.08$ and to its harmonics $2f, 3f, 4f \ldots$.

To characterize the chaotic dynamics quantitatively, we calculate the Lyapunov exponents. For time-delay systems, a complete spectrum of Lyapunov exponents contains an infinite number of terms, although in order to properly judge on the relevant characteristics of the attractor we need only some restricted number of the largest ones. To evaluate them we use a kind of Benettin method [Benettin *et al.*, 1980; Shimada & Nagashima, 1979; Pikovsky & Politi, 2016], adapted for time-delay systems [Farmer, 1982; Yanchuk & Giacomelli, 2017; Balyakin & Ryskin, 2007; Koloskova *et al.*, 2018]. The content of the procedure is the simultaneous integration of Eq. (9) together with a set of linearized variation equations

$$\ddot{\tilde{x}} + [d(t) - a + 3b\dot{x}^2]\dot{\tilde{x}} + \tilde{x}\cos x = \varepsilon[\dot{\tilde{x}}(t-\tau) - \dot{\tilde{x}}], \tag{14}$$

the number of which corresponds to the number of the required Lyapunov exponents.

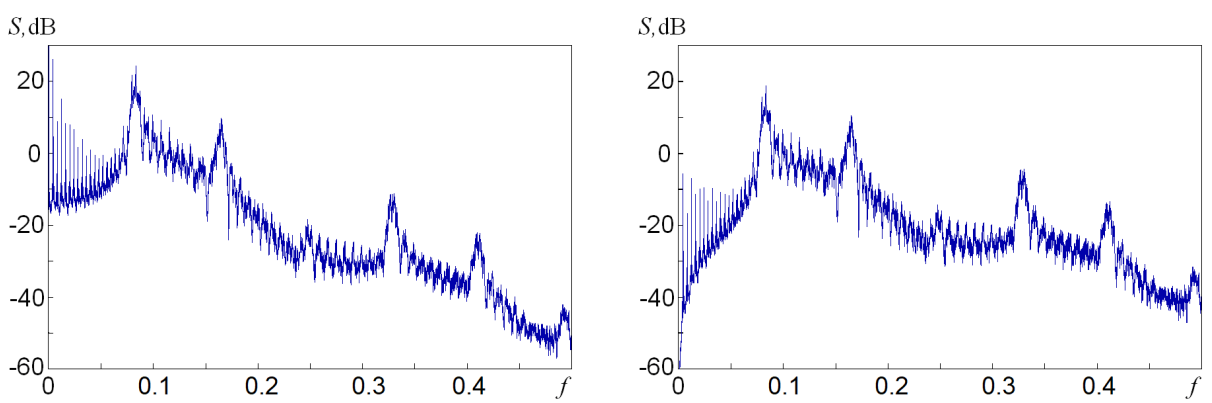

(a) (b)

Fig. 6. Power spectra corresponding to the dynamical variables x and $\dot{x}$ in the chaotic regime associated with the Smale–Williams attractor and obtained by processing data of numerical integration of Eq. (9). Parameters are assigned in accordance with (13).

The perturbation vectors related to a time instant nT, where T is the modulation period, are determined by a set of quantities $\tilde{x}(nT)$, $\dot{\tilde{x}}(nT)$ and functions $\dot{\tilde{x}}(t)$, $t \in [nT - \tau, nT)$. At each period T the resulting vectors are subjected to the Gram–Schmidt orthogonalization procedure and renormalized so that the norms of the vectors turn out to be unit. The Lyapunov exponents are estimated as average rates of increase (decrease) of cumulative sums of logarithms of norms for perturbation vectors after orthogonalization, but before normalization.

The calculation of the largest three Lyapunov exponents of the Poincaré map for the attractor at the given parameters (13) yields

$$\Lambda_1 = 0.650, \quad \Lambda_2 = -6.325, \quad \Lambda_3 = -7.061, \ldots . \tag{15}$$

The positive value of the first exponent indicates the chaotic nature of the dynamics, and, as we can see, it is quite close to the value $\ln 2 = 0.693\ldots$ that corresponds to the Bernoulli map of Fig. 1(b). The Kaplan–Yorke dimension estimated from the spectrum of Lyapunov exponents [Kaplan & Yorke, 1979; Farmer *et al.*, 1983] for this attractor is $D = 1 + \Lambda_1/|\Lambda_2| \approx 1.10$.

5. The Dependence of the Dynamics on the Parameters

Our consideration in the previous section relates to a particular selected point in the parameter space, where the hyperbolic attractor in the form of Smale–Williams solenoid takes place for the Poincaré map. Now we are going to discuss how the dynamics depend on the parameters. It is rather difficult to get a comprehensive picture, since the number of parameters in the model is quite large. Nevertheless, the content presented below will illustrate several important aspects. Firstly, we will try to give a general idea about the nature of the dynamical behavior, including its various types, consisting of regular and chaotic regimes subdivided to oscillatory and rotational ones that are specific to the systems with sine nonlinearity. Secondly, it will illustrate and demonstrate to a certain extent the inherent property of structural stability, which is expressed by the fact that the hyperbolic chaos occupies continuous regions in the parameter space. Thirdly, it is interesting to see how the regions of hyperbolic chaos can be disposed in the parameter space and what are the possible scenarios arising of hyperbolic chaos as we move towards these regions under parameter variation, which may be useful for orientation in general when searching for situations with structurally stable chaos in various systems of natural or technical origin.

We will use a technique of representing the numerical results of the dynamics analysis with charts of dynamical regimes [Kuznetsov *et al.*, 1996; Stoop *et al.*, 2012; Doroshenko *et al.*, 2014]. To build a chart, two parameters are selected, which will be varied during the calculations while other parameters are fixed. Then, the plane of parameters is scanned providing numerical integration of the dynamical equations (9) at the grid nodes with a certain step in two parameters. For each node of the grid we produce about 10^3 iterations of the Poincaré map, and a type of the dynamical regime is identified based on the results of the calculations. The diagnostics is executed, firstly, on the basis of the calculation of the largest Lyapunov exponent: its positive value implies chaos; zero corresponds to quasiperiodic dynamics, and negative values correspond to periodic movements. In the latter case, the repetition period of the system states is determined (from one to 14 iterations of the Poincaré map), with some initially defined level of allowable error. For chaotic regimes, a specially developed data processing algorithm is additionally applied, which allows confirming or rejecting the assumption that the map for the angular variable transformation on the modulation period belongs to the same topological class as the double expanding circle map. This allows distinguishing regimes where chaos corresponds to the Smale–Williams solenoid.[1]

[1]The algorithm consists in analyzing the coarsened dependence of the values of phases φ_n versus φ_{n-1} obtained on successive modulation periods and defined on a unit interval, as described in the previous section. The values φ_{n-1} recorded for the considered regime for N consecutive modulation periods are grouped into "boxes", each of which occupies $1/K$ of the full interval. The value of the coarsened function f_k is taken as an average value $\exp(2\pi i\varphi_n)$ over all φ_{n-1} that falls into this box. According to the data obtained, from $k = 0$ to $K - 1$, step by step, the phase increment $\sum \arg f_k$ in the full interval is calculated, and it is verified that it is either equal to two or not. Also, the monotony of the coarsened phase depending on k is checked. If both of these conditions are true, the pixel on the chart is marked as referring to the situation of the presence of the Smale–Williams attractor.

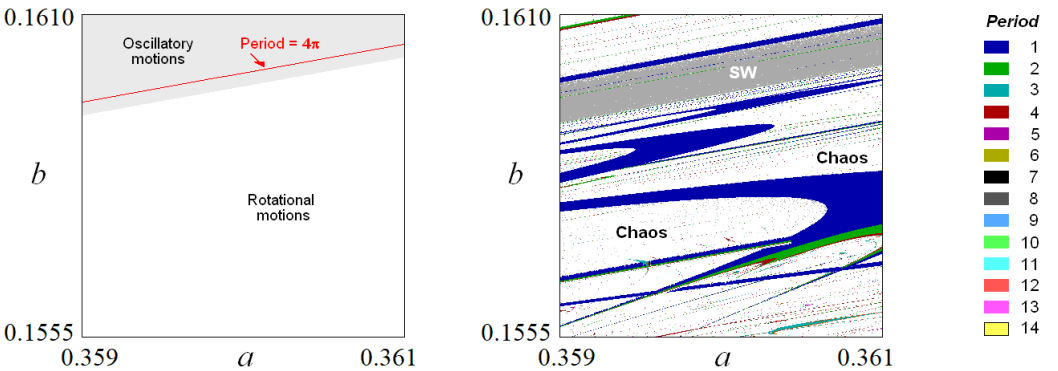

Fig. 7. (a) Regions of oscillatory and rotational motions for the reduced system (11) on the plane of parameters (a, b) with $d = 0$ and (b) the chart of regimes for the system (9) on the same plane of parameters, where areas of chaos and of periodic motions are shown. The region of hyperbolic chaos associated with the Smale–Williams attractor is shown in gray and is marked as SW, other chaotic regimes are shown in white. The legend for periodic regimes is shown on the right, where the periods are indicated in units of the period of braking and activity of the pendulum. Fixed parameters are $\mu = 0.087$, $\varepsilon = 0.0003$, $D = 0.8$, $T = 250$, $T_0 = T/4$, $\tau = T/2$.

In accordance with the diagnostics, a corresponding pixel in the diagram is indicated by a certain color, and we move on to the analysis of the next point of the parameter plane. Note that it is reasonable to set the state obtained as a final system state at the previous point as the initial state to start the computations at the new point, which in most cases accelerates the convergence to the sustained dynamics ("scanning with inheritance").

As an initial step in our analysis, Fig. 7(a) shows a diagram on the plane of parameters (a, b) for the conventional Froude pendulum described by Eq. (11) with $d = 0$ and $\mu = 0.087$, where the areas of oscillatory and rotational regimes are indicated, and the red line corresponds to the relaxation self-oscillations at a frequency equal to a half of the frequency of small oscillations of the pendulum. In Fig. 7(b) on the plane of the same parameters, a chart of regimes for the system (9) is shown. We can see zones of periodic and chaotic dynamics located both in the regions of oscillatory and of rotational movements. Chaotic attractors in the form of a Smale–Williams solenoid in the Poincaré map take place in the SW region, which is a strip shown in gray in the diagram. The center of this strip corresponds to the half-frequency red line in Fig. 7(a).

Figure 8 shows a chart of regimes on the parameter plane (ε, D), i.e. the time-delay feedback intensity parameter versus the dissipation parameter introduced by the brake pad during the braking stages. Herewith, the remaining parameters correspond to the situation when the period of relaxation self-oscillations at the activity stage is exactly twice the period of small oscillations. The structure of the regions is determined by the character of the excitation transfer from one stage of activity to the next in the course of the system operation, as discussed in Sec. 4. In the central part of the chart one can see a broad area SW, where hyperbolic chaos takes place. Exiting this area corresponds to the fact that the dissipation at the stages of breaking decreases and becomes too small to provide a

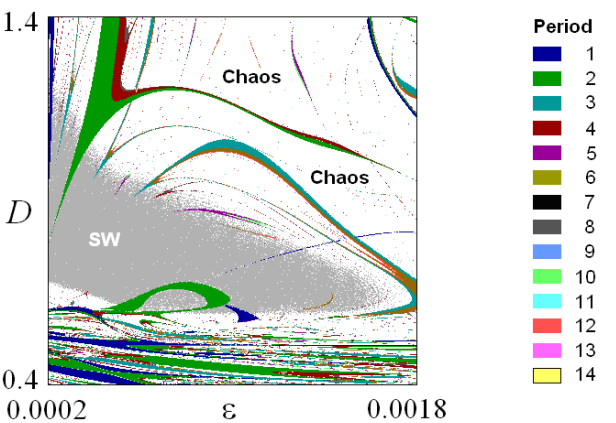

Fig. 8. Chart of regimes of the system (9) on the plane ε–D, where areas of chaos and of periodic motions are shown. The region of hyperbolic chaos associated with the Smale–Williams attractor is shown in gray and marked as SW, other chaotic regimes are shown in white. The legend for periodic regimes is shown on the right. Fixed parameters are $a = 0.36, b = 0.16, \mu = 0.087, \varepsilon = 0.0003, D = 0.8, T = 250$, $T_0 = T/4, \tau = T/2$.

sufficient degree of damping of the natural oscillations of the pendulum after the previous activity stage, which makes a competing contribution to the stimulation of the oscillatory process at the new activity stage, so that the phase doubling transfer mechanism is violated. The exit through the upper boundary of the SW region corresponds to the fact that at the curve representing the graph for the phases, a bend is formed on one of the branches, and then a maximum and a minimum appear, so that the monotony property is lost. (This means that when a stretched double loop is inserted into the original toroidal region in the solenoid construction procedure, there appears a local fold on the loop, which leads to disruption of the proper solenoid structure.) When the parameters at the upper edge

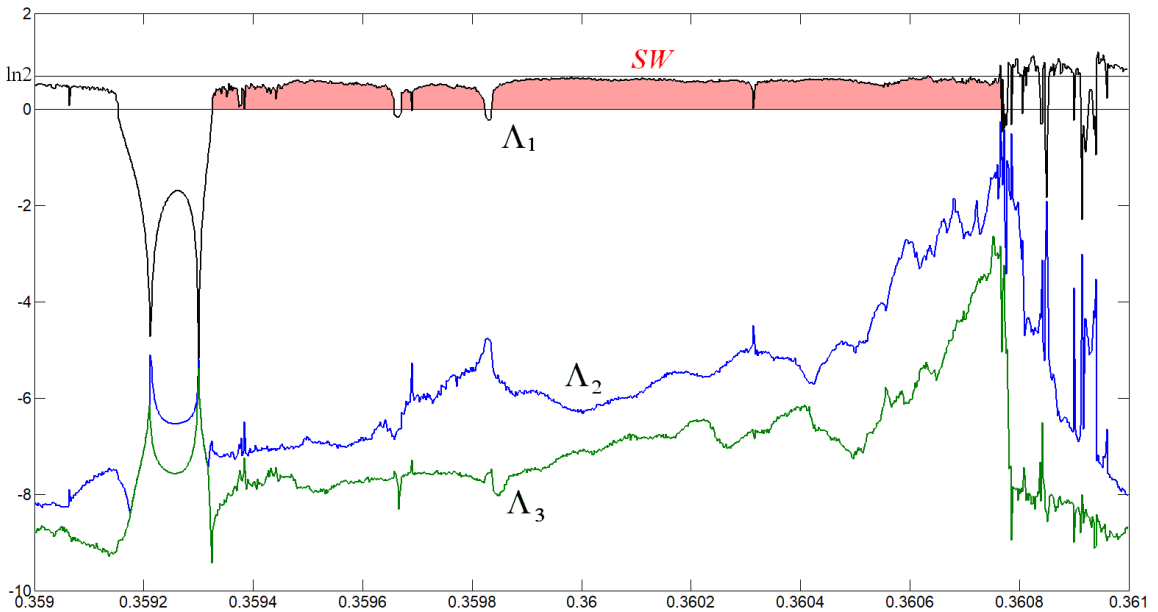

(a)

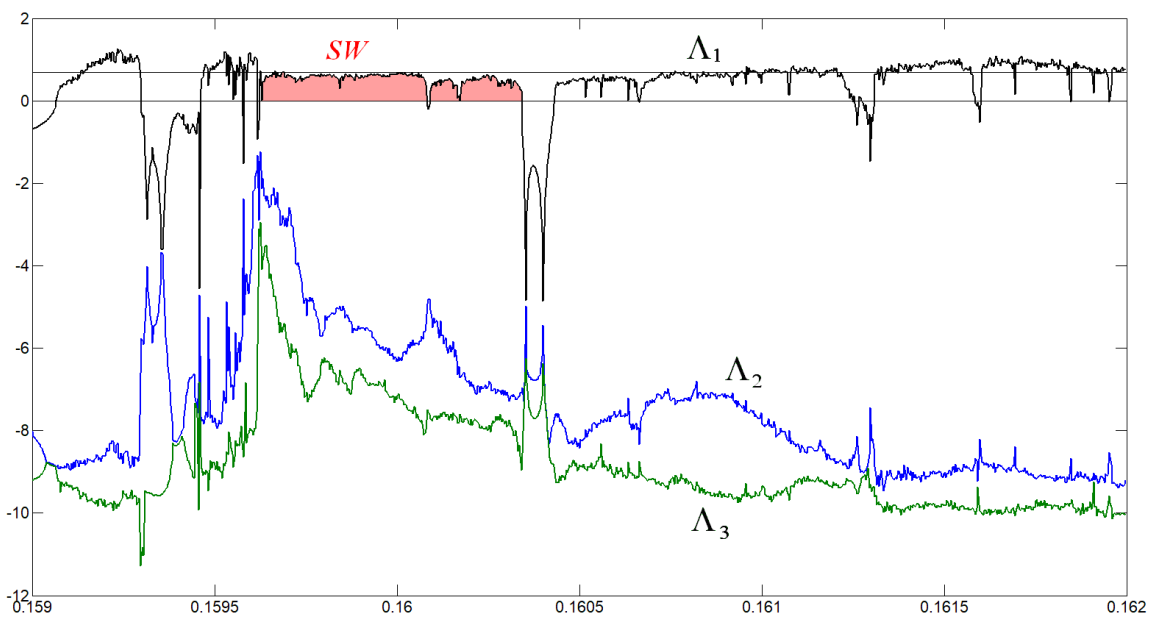

(b)

Fig. 9. Spectrum of Lyapunov exponents of model (9): (a) depending on the parameter a at $b = 0.16$ and (b) depending on b at $a = 0.36$. The remaining parameters are $\mu = 0.087, \varepsilon = 0.0003, D = 0.8, T = 250, T_0 = T/4, \tau = T/2$.

of the region SW are varied, periodic motions become possible; on the chart one can see there a set of periodicity tongues. Visually, they look similar to the classical synchronization Arnold tongues [Boyland, 1986; de Figueiredo & Malta, 1998], but the principal difference from the classical picture is that between them we have chaotic dynamics rather than the quasiperiodicity.

A characteristic feature of the "fragile chaos" is that within the corresponding areas shown in white, local formations occur corresponding to the periodic dynamics called "shrimps" [Stoop *et al.*, 2012] and their "mustaches", the filaments emanating from each shrimp, which are narrow bands of periodicity running through the region of chaos. Their presence just indicates violation of the robustness. Such formations are absent in the area of hyperbolic chaos SW, although when approaching its borders one can observe the appearance of local zones of regular dynamics in the form of the above mentioned tongues.

The fact that the hyperbolic chaos occupies a continuous region in the parameter space is consistent with the theoretical concept of the inherent structural stability. Detailed consideration of the scenarios for the destruction of hyperbolic chaos is beyond the scope of this paper; for the discussion of some results in the context of this problem, see [Isaeva *et al.*, 2012; Isaeva *et al.*, 2013; Isaeva *et al.*, 2015].

Figure 9 shows the dependences of three Lyapunov exponents on parameters a and b, corresponding to paths on the chart of Fig. 7(b) along two lines crossing at the hyperbolic chaos point $a = 0.36$, $b = 0.16$, respectively, in horizontal and vertical directions. Parameter intervals where the analysis of the properties of the map for the phases reveals the topology corresponding to the Smale–Williams attractor, are marked with pink background under the plot of the largest exponent. Its values in these regions are roughly estimated from above by the value of $\ln 2$, although at some places they drop to notably smaller values. The property of structural stability of the hyperbolic attractor is manifested in the fact that it persists in the continuous parameter intervals, and the dependence of the Lyapunov exponent on a parameter is quite smooth. In the areas of "fragile chaos", the dependence of the Lyapunov exponent on a parameter is characterized by a strong irregularity, and by dips to negative values corresponding to the so-called "periodicity windows" that are characteristic of nonhyperbolic chaos, which on the chart of regimes correspond to the intersections of the "shrimps" and their "mustaches".

6. Verifying the Hyperbolicity of Attractors in the Time-Delay System. The "Criterion of Angles"

One of the methods for testing hyperbolicity [Lai *et al.*, 1993; Anishchenko *et al.*, 2000] is that for a typical trajectory belonging to the invariant set under consideration, the equations in variations for the perturbation vectors are solved first in forward time to determine the unstable subspace and then in reverse time to determine the stable subspace. Further, for the set of points of the trajectory, the angles between these subspaces are calculated, and the nature of the distribution of the angles is analyzed. If it is separated from zero angles, then this indicates the hyperbolic nature of the invariant set, whereas the occurrence of angles close to zero indicates the absence of hyperbolicity. This method has shown its effectiveness in recognizing hyperbolic and nonhyperbolic chaos in many particular systems [Kuznetsov, 2005; Kuznetsov & Seleznev, 2006; Kuznetsov & Kruglov, 2017]. For the attractor of the system of two alternately excited Froude pendulums, this method was applied in [Kuznetsov & Kruglov, 2019].

In the case of time-delay systems, the problem is that the dimensions of the phase space and, accordingly, of the contracting subspace are infinite. This problem can be overcome with the help of a variant of the method, where vectors that belong to the contracting subspace are not used to identify this subspace, but vectors defining its orthogonal complement, the dimension of which is usually small [Kuptsov, 2012; Kuptsov & Kuznetsov, 2016]. These vectors are obtained from the solution of the adjoint linearized equations; the method of their derivation for systems with one or several delay times was specified in [Kuptsov & Kuznetsov, 2016, 2018].

For our system (9) the equations in variations near the reference phase trajectory can be rewritten as

$$\begin{aligned} \dot{\tilde{x}} &= \tilde{u}, \\ \dot{\tilde{u}} &= -[d(t) - a + \varepsilon + b\dot{x}^2]\tilde{u} \\ &\quad - \tilde{x}\cos x + \varepsilon\tilde{u}(t-\tau). \end{aligned} \tag{16}$$

The adjoint system is constructed as suggested in [Kuptsov & Kuznetsov, 2016, 2018], and is a system of equations with deviating argument of the advanced type

$$\begin{aligned}\dot{\tilde{y}} &= \tilde{v}\cos x,\\ \dot{\tilde{v}} &= -y + [d(t) - a + \varepsilon + b\dot{x}^2]\tilde{v}\\ &\quad - \varepsilon\tilde{v}(t+\tau).\end{aligned} \tag{17}$$

These equations are constructed so that the inner product for the vectors given by (16) and (17) defined as

$$\begin{aligned}\mathbf{x}\cdot\mathbf{y} &= \tilde{x}(t)\tilde{y}(t) + \tilde{u}(t)\tilde{v}(t)\\ &\quad + \varepsilon\int_{t-\tau}^{t}\tilde{u}(\theta)\tilde{v}(\tau+\theta)d\theta,\end{aligned} \tag{18}$$

remains constant in time.

In the region of parameters of our interest, the unstable subspaces of the trajectories belonging to the attractor are one-dimensional, and the same is true for the orthogonal complement to the stable

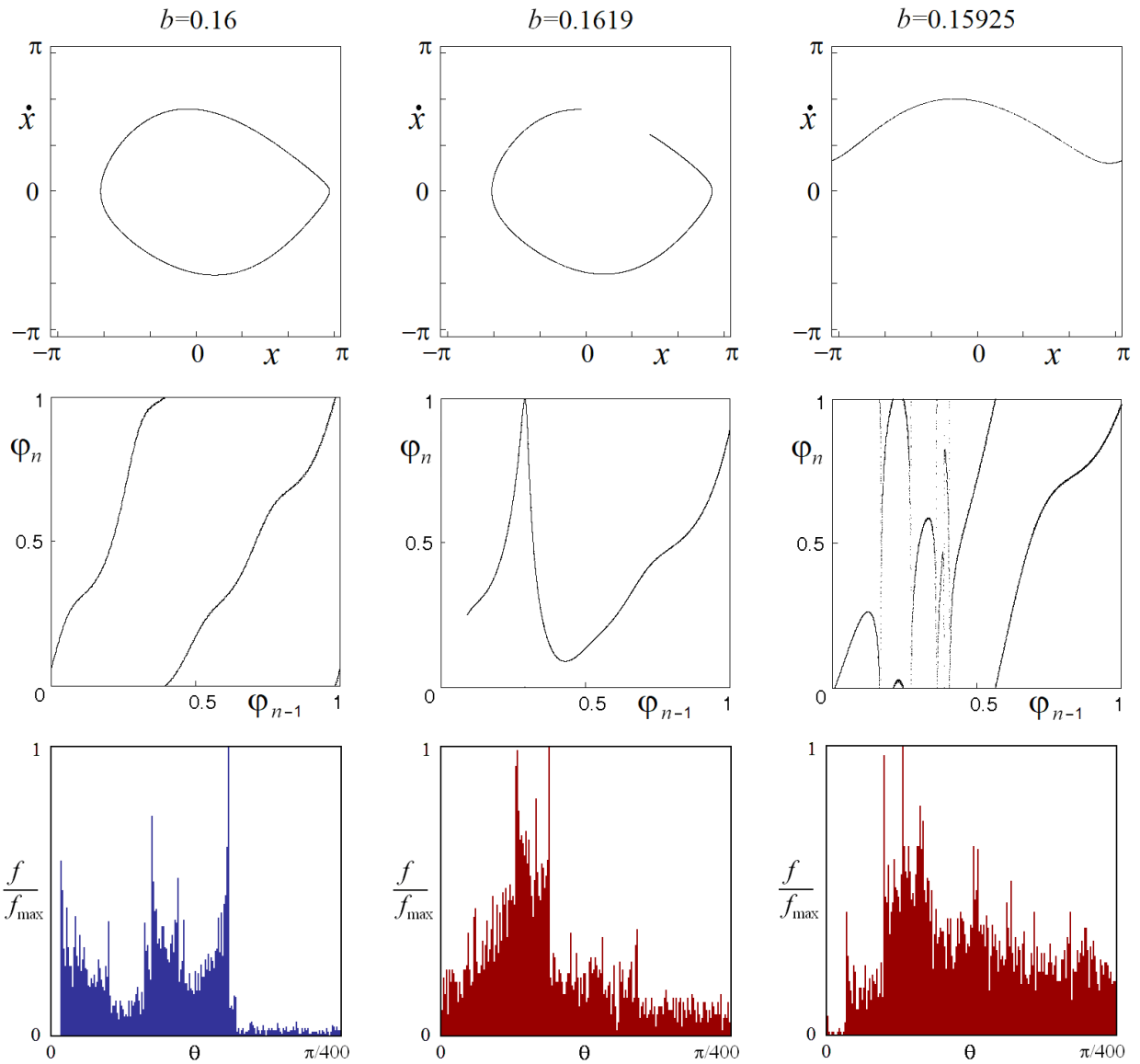

Fig. 10. Portraits of attractors in the Poincaré section (upper row), diagrams for phases at successive periods of activity and suppression (middle row) and histograms of the intersection angles of stable and unstable subspaces for the perturbation vectors plotted for checking hyperbolicity by the criterion of angles (bottom row). The values of the parameter b are indicated by inscriptions, and the remaining parameters are assigned according to (13). The left column corresponds to a hyperbolic attractor, and the central and right columns correspond to nonhyperbolic attractors of oscillatory and rotational types respectively.

subspaces. The procedure is to calculate first a long segment of reference trajectory of the system (9), with simultaneous integration of the equations in variations (16), giving a set of vectors associated with positive Lyapunov exponent and belonging to the unstable subspace. Further, in reverse time, the integration of the adjoint system is carried out along the same trajectory. (Although in its formal record (17) it is of advanced type, in the inverse time the solutions behave as for a retarded type system, so that troubles concerning the mathematical nature of the advanced type equations do not arise.) At the end of the procedure, the angles are calculated using the scalar product (18) for pairs of vectors belonging to identical points of the reference trajectory at different times, and a histogram of their distribution is plotted.

Figure 10 illustrates the results of checking the hyperbolicity of attractors for the system (9). The left column corresponds to the hyperbolic attractor discussed in Sec. 4, and the central and right columns correspond to nonhyperbolic attractors, which arise with a shift in the parameter b.

The top row shows stroboscopic portraits of the attractors. As can be seen, the left and central plots relate to the oscillatory type of motion, and the right plot to the rotational one. Lyapunov exponents for the hyperbolic attractor were indicated in Sec. 4, and for the nonhyperbolic attractors they are $\Lambda = \{0.766, -9.141, -9.838\}$ and $\Lambda = \{0.959, -8.606, -9.485\}$, respectively. Their Kaplan–Yorke dimensions $D_{\mathrm{KY}} = 1 + \Lambda_1/|\Lambda_2|$ are approximately 1.08 and 1.10.

The middle row shows diagrams for oscillation phases at successive modulation stages, calculated according to the procedure explained in Sec. 4. As one can see, only the left diagram corresponds to the topological type of the Bernoulli map, while diagrams for nonhyperbolic attractors clearly do not belong to this type.

The bottom row shows histograms of the intersection angles of stable and unstable subspaces for trajectories on the attractors. The left diagram clearly shows that the distribution is separated from zero angles, which confirms the hyperbolic nature of the attractor of the Poincaré map. Similar results are obtained when the parameters of the system vary in a quite wide range (SW region in Figs. 7 and 8), which correspond to the roughness property (structural stability) inherent to the hyperbolic attractor. The central and right histograms indicate the presence of angles close to zero between vectors belonging to the stable and unstable subspaces; thus implying the nonhyperbolic nature of the attractors.

7. Conclusion

In this paper, the occurrence of rough hyperbolic chaos associated with the Smale–Williams attractor is established for a system based on the Froude pendulum supplemented by time-delay feedback and with periodic externally forced alternating excitation and suppression of activity due to periodic braking of the oscillations.

The mathematical model is formulated and its numerical research is carried out. Areas of chaotic and regular dynamics are identified in the parameter space using the analysis of periodicity and calculations of Lyapunov exponents. It is shown that with the appropriate specification of the parameters, the attractor of the stroboscopic Poincaré map is a Smale–Williams solenoid, the nature of which is confirmed by checking the topological nature of the map for the angular variable, executed visually or automatically using a specially developed algorithm. The hyperbolicity of the chaotic attractor was also confirmed by using a criterion based on the analysis of the intersection angles of stable and unstable invariant subspaces of small perturbation vectors and checking for the absence of tangencies between these subspaces. The structure of the system parameter space was studied; in particular, charts of regimes were presented in two-dimensional sections of the parameter space, which allowed judging on the location of the regions of hyperbolic chaos, which occupy continuous zones due to its inherent structural stability, and on the nature of the dynamics in the adjacent regions.

The proposed system, obviously, allows implementation in the form of a specific mechanical device, which would enable experimental studies of hyperbolic chaos. Due to the visibility of the dynamics of the system, which is a mechanical object, this kind of experiment could be useful in practical laboratory classes for undergraduate and graduate students specializing in nonlinear dynamics.

The considered approach can serve as an example for constructing objects of different natures, manifesting hyperbolic attractors on a base of systems, in which oscillatory excitation is

transmitted between successive stages of activity in a resonant manner due to the difference in the frequencies of small and large oscillations by an integer number of times. The scheme turns out to be structurally simpler than many previously proposed versions of systems with time-delay, demonstrating hyperbolic chaos [Kuznetsov & Ponomarenko, 2008; Kuznetsov & Pikovsky, 2008; Baranov *et al.*, 2010; Arzhanukhina & Kuznetsov, 2014], due to the absence of an auxiliary signal source at a frequency close to the natural frequency of the oscillator or of additional feedback circuits.

Our system based on the Froude pendulum, can be interpreted as an example of the application of the control technique associated with a use of time-delay feedback to obtain a specific phenomenon of nonlinear dynamics, namely, the robust hyperbolic chaos in our case. As can be presumed, in the context of mechanical systems this direction can be interesting, say, for robotic devices, in the perspective of controlling them with the involvement of chaos control ideas [Schöll & Schuster, 2008].

Taking into account the analogy of pendulum systems with systems based on Josephson junctions and on phase-locked loops, the considered model can serve as a sample for constructing electronic analogs functioning as chaos generators, where roughness due to the hyperbolic nature of the attractor will be an important advantage in the context of possible information and communication applications.

The presented material is interesting with respect to the physical content of the hyperbolic theory that is a deeply developed and advanced section of the modern theory of dynamical systems, which gives a rigorous justification for the presence of chaos characterized by the property of structural stability.

Acknowledgments

Development of the operating principle of the system, construction of the mathematical model and verification of hyperbolicity were carried out under support of the grant of Russian Science Foundation No. 15-12-20035 (S. P. Kuznetsov, Secs. 2, 3 and 6). Numerical calculations demonstrating the hyperbolic attractor, as well as a study of the dependences of dynamical behaviors on parameters were carried out under support of the grant of Russian Science Foundation No. 17-12-01008 (Yu. V. Sedova, Secs. 4 and 5).

References

Anishchenko, V. S., Kopeikin, A. S., Kurths, J., Vadivasova, T. E. & Strelkova, G. I. [2000] "Studying hyperbolicity in chaotic systems," *Phys. Lett. A* **270**, 108–119.

Anosov, D. V., Gould, G. G., Aranson, S. K., Grines, V. Z., Plykin, R. V., Safonov, A. V., Sataev, E. A., Shlyachkov, S. V., Solodov, V. V., Starkov, A. N. & Stepin, A. M. [1995] *Dynamical Systems IX*: *Dynamical Systems with Hyperbolic Behaviour*, Encyclopaedia of Mathematical Sciences, Vol. 66 (Springer).

Arzhanukhina, D. S. & Kuznetsov, S. P. [2014] "Robust chaos in autonomous time-delay system," *Izvestiya VUZ*, *Appl. Nonlin. Dyn.* **22**, 36–49.

Balyakin, A. A. & Ryskin, N. M. [2007] "Peculiarities of calculation of the Lyapunov exponents set in distributed self-oscillated systems with delayed feedback," *Izvestiya VUZ*, *Appl. Nonlin. Dyn.* **15**, 3–21 (in Russian).

Banerjee, S., Yorke, J. A. & Grebogi, C. [1998] "Robust chaos," *Phys. Rev. Lett.* **80**, 3049.

Baranov, S. V., Kuznetsov, S. P. & Ponomarenko, V. I. [2010] "Chaos in the phase dynamics of q-switched van der Pol oscillator with additional delayed feedback loop," *Izvestiya VUZ*, *Appl. Nonlin. Dyn.* **18**, 12–23 (in Russian).

Bellman, R. E. & Cooke, K. L. [2012] *Differential-Difference Equations* (Academic Press).

Benettin, G., Galgani, L., Giorgilli, A. & Strelcyn, J. M. [1980] "Lyapunov characteristic exponents for smooth dynamical systems and for Hamiltonian systems; A method for computing all of them. Part 1: Theory," *Meccanica* **15**, 9–20.

Best, R. E. [2007] *Phase-Locked Loops*: *Design*, *Simulation and Applications* (McGraw Hill Professional).

Boyland, P. L. [1986] "Bifurcations of circle maps: Arnol'd tongues, bistability and rotation intervals," *Commun. Math. Phys.* **106**, 353–381.

Cao, H., Chi, X. & Chen, G. [2004] "Suppressing or inducing chaos by weak resonant excitations in an externally-forced Froude pendulum," *Int. J. Bifurcation and Chaos* **14**, 1115–1120.

Cuevas-Maraver, J., Kevrekidis, P. G. & Williams, F. (eds.) [2014] *The Sine-Gordon Model and Its Applications*: *From Pendula and Josephson Junctions to Gravity and High-Energy Physics* (Springer).

Dai, L. & Singh, M. C. [1998] "Periodic, quasiperiodic and chaotic behavior of a driven Froude pendulum," *Int. J. Non-Lin. Mech.* **33**, 947–965.

de Figueiredo, J. B. & Malta, C. P. [1998] "Lyapunov graph for two-parameters map: Application to the circle map," *Int. J. Bifurcation and Chaos* **8**, 281–293.

Dmitriev, A. S., Efremova, E. V., Maksimov, N. A. & Panas, A. I. [2012] *Generation of Chaos* (Technosfera, Moscow) (in Russian).

Doroshenko, V. M., Emelianova, Yu. P., Kuznetsov, A. P. & Sedova, Yu. V. [2014] "A method of Lyapunov charts: Illustrations to the theory of coupled self-oscillating systems," *Vestnik Saratovskogo Gosudaratvennogo Tekhnicheskogo Universiteta* **74**, 12–22 (in Russian).

Doroshenko, V. M., Kruglov, V. P. & Kuznetsov, S. P. [2018] "Smale–Williams solenoids in a system of coupled Bonhoeffer–van der Pol oscillators," *Russ. J. Nonlin. Dyn.* **14**, 435–451.

Elhadj, Z. & Sprott, J. C. [2011] *Robust Chaos and Its Applications* (World Scientific, Singapore).

El'sgol'ts, L. E. & Norkin, S. B. [1973] *Introduction to the Theory and Application of Differential Equations with Deviating Arguments* (Academic Press).

Farmer, J. D. [1982] "Chaotic attractors of an infinite-dimensional dynamical system," *Physica D* **4**, 366–393.

Farmer, J. D., Ott, E. & Yorke, J. A. [1983] "The dimension of chaotic attractors," *Physica D* **7**, 153–180.

Gusso, A., Dantas, W. G. & Ujevic, S. [2019] "Prediction of robust chaos in micro and nanoresonators under two-frequency excitation," *Chaos* **29**, 033112.

Isaeva, O. B., Kuznetsov, S. P. & Sataev, I. R. [2012] "A 'saddle-node' bifurcation scenario for birth or destruction of a Smale–Williams solenoid," *Chaos* **22**, 043111.

Isaeva, O. B., Kuznetsov, S. P., Sataev, I. R. & Pikovsky, A. [2013] "On a bifurcation scenario of a birth of attractor of Smale–Williams type," *Russ. J. Nonlin. Dyn.* **9**, 267–294 (in Russian).

Isaeva, O. B., Kuznetsov, S. P., Sataev, I. R., Savin, D. V. & Seleznev, E. P. [2015] "Hyperbolic chaos and other phenomena of complex dynamics depending on parameters in a nonautonomous system of two alternately activated oscillators," *Int. J. Bifurcation and Chaos* **25**, 1530033-1–15.

Jenkins, G. M. & Watts, D. G. [1968] *Spectral Analysis and Its Applications*, Time Series Analysis (Holden-Day, San Francisco).

Kaplan, J. L. & Yorke, J. A. [1979] "A chaotic behavior of multi-dimensional differential equations," *Functional Differential Equations and Approximations of Fixed Points*, Lecture Notes in Mathematics, Vol. 730, eds. Peitgen, H.-O. & Walther, H.-O. (Springer, Berlin, NY), pp. 204–227.

Katok, A. & Hasselblatt, B. [1995] *Introduction to the Modern Theory of Dynamical Systems* (Cambridge University Press).

Koloskova, A. D., Moskalenko, O. I. & Koronovskii, A. A. [2018] "A method for calculating the spectrum of Lyapunov exponents for delay systems," *Tech. Phys. Lett.* **44**, 374–377.

Kuptsov, P. V. [2012] "Fast numerical test of hyperbolic chaos," *Phys. Rev. E* **85**, 015203.

Kuptsov, P. V. & Kuznetsov, S. P. [2016] "Numerical test for hyperbolicity of chaotic dynamics in time-delay systems," *Phys. Rev. E* **94**, 010201.

Kuptsov, P. V. & Kuznetsov, S. P. [2018] "Numerical test for hyperbolicity in chaotic systems with multiple time delays," *Commun. Nonlin. Sci. Numer. Simulat.* **56**, 227–239.

Kuznetsov, A. P., Kuznetsov, S. P., Sataev, I. R. & Chua, L. O. [1996] "Multi-parameter criticality in Chua's circuit at period-doubling transition to chaos," *Int. J. Bifurcation and Chaos* **6**, 119–148.

Kuznetsov, S. P. [2005] "Example of a physical system with a hyperbolic attractor of the Smale–Williams type," *Phys. Rev. Lett.* **95**, 144101.

Kuznetsov, S. P. & Seleznev, E. P. [2006] "A strange attractor of the Smale–Williams type in the chaotic dynamics of a physical system," *J. Exp. Theoret. Phys.* **102**, 355–364.

Kuznetsov, S. P. & Pikovsky, A. S. [2008] "Hyperbolic chaos in the phase dynamics of a Q-switched oscillator with delayed nonlinear feedbacks," *Europhys. Lett.* **84**, 10013.

Kuznetsov, S. P. & Ponomarenko, V. I. [2008] "Realization of a strange attractor of the Smale–Williams type in a radiotechnical delay-fedback oscillator," *Tech. Phys. Lett.* **34**, 771–773.

Kuznetsov, S. P. [2011] "Dynamical chaos and uniformly hyperbolic attractors: From mathematics to physics," *Phys.-Uspekhi* **54**, 119–144.

Kuznetsov, S. P. [2012] *Hyperbolic Chaos*: *A Physicist's View* (Higher Education Press, Beijing and Springer-Verlag, Berlin, Heidelberg).

Kuznetsov, S. P. & Kruglov, V. P. [2017] "On some simple examples of mechanical systems with hyperbolic chaos," *Proc. Steklov Instit. Math.* **297**, 208–234.

Kuznetsov, S. P. & Kruglov, V. P. [2019] "Hyperbolic chaos in a system of two Froude pendulums with alternating periodic braking," *Commun. Nonlin. Sci. Numer. Simulat.* **67**, 152–161.

Kuznetsov, S. P. & Sedova, Y. V. [2019] "Hyperbolic chaos in the Bonhoeffer–van der Pol oscillator with additional delayed feedback and periodically modulated excitation parameter," *Izvestiya VUZ, Appl. Nonlin. Dyn.* **27**, 77–95 (in Russian).

Lai, Y. C., Grebogi, C., Yorke, J. A. & Kan, I. [1993] "How often are chaotic saddles nonhyperbolic?" *Nonlinearity* **6**, 779–797.

Landa, P. S. [2013] *Nonlinear Oscillations and Waves in Dynamical Systems* (Springer Science & Business Media).

Likharev, K. K. [1986] *Dynamics of Josephson Junctions and Circuits* (CRC Press).

Pikovsky, A. & Politi, A. [2016] *Lyapunov Exponents*: *A Tool to Explore Complex Dynamics* (Cambridge University Press).

Pugh, C. & Peixoto, M. M. [2008] "Structural stability," *Scholarpedia* **3**, 4008.

Rabinovich, M. I. & Trubetskov, D. I. [2012] *Oscillations and Waves*: *In Linear and Nonlinear Systems* (Springer Science & Business Media).

Rayleigh, J. W. S. & Lindsay, R. B. [1945] *The Theory of Sound* (Courier Corporation).

Schöll, E. & Schuster, H. G. [2008] *Handbook of Chaos Control* (John Wiley & Sons).

Shilnikov, L. [1997] "Mathematical problems of nonlinear dynamics: A tutorial," *Int. J. Bifurcation and Chaos* **7**, 1953–2001.

Shimada, I. & Nagashima, T. [1979] "A numerical approach to ergodic problem of dissipative dynamical systems," *Progr. Theoret. Phys.* **61**, 1605–1616.

Smale, S. [1967] "Differentiable dynamical systems," *Bull. Amer. Math. Soc.* **73**, 747–817.

Stoop, R., Martignoli, S., Benner, P., Stoop, R. L. & Uwate, Y. [2012] "Shrimps: Occurrence, scaling and relevance," *Int. J. Bifurcation and Chaos* **22**, 1230032-1–14.

Strelkov, S. P. [1933] "The Froude pendulum," *Zh. Tekh. Fiz.* **3**, 563–573.

Sveshnikov, A. A. [2014] *Applied Methods of the Theory of Random Functions* (Elsevier).

Yanchuk, S. & Giacomelli, G. [2017] "Spatio-temporal phenomena in complex systems with time delays," *J. Phys. A*: *Math. Theoret.* **50**, 103001.